Supplemental material

Albarran-Juarez et al., https://doi.org/10.1084/jem.20180483

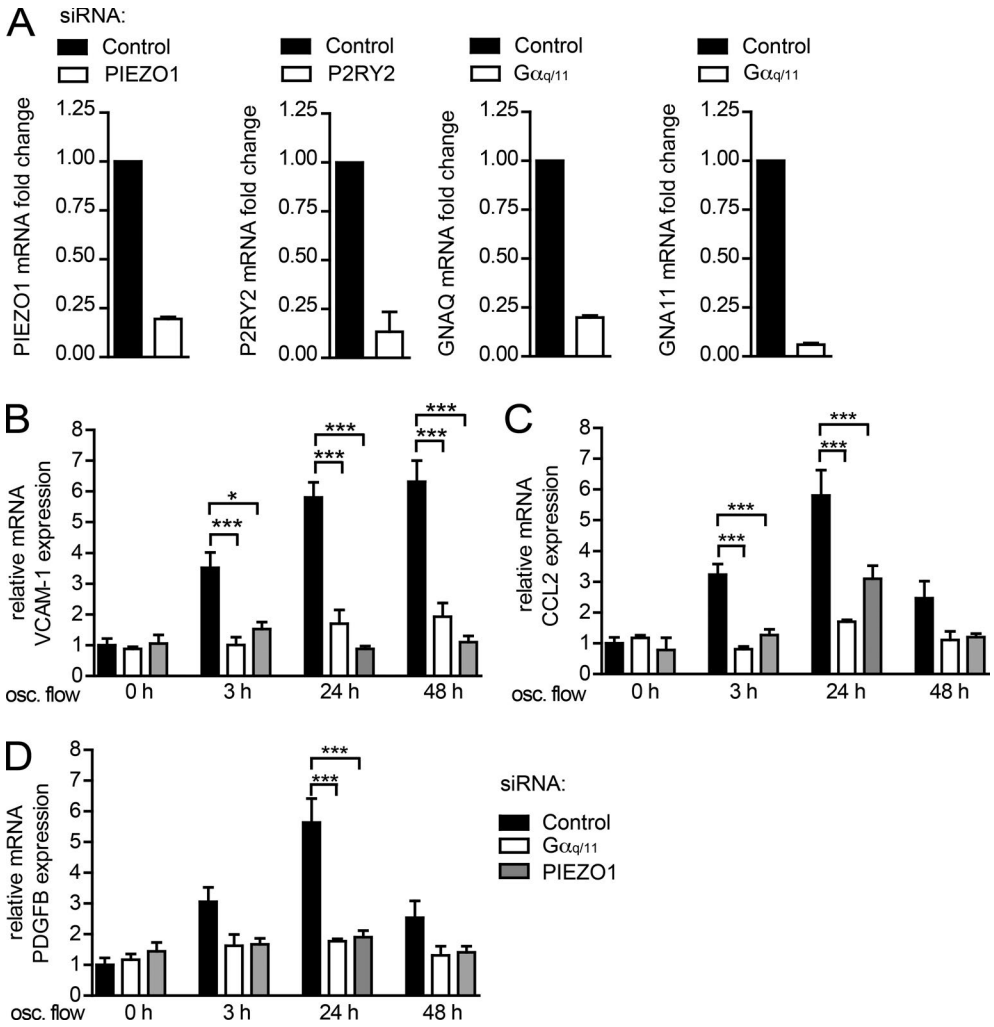

Figure S1. **Knock-down efficiency of $G\alpha_q$, $G\alpha_{11}$, $P2Y_2$, and Piezo1 in HUAECs and expression of inflammatory markers upon disturbed flow. (A)** Quantitative RT-PCR was performed 48 h after the second siRNA transfection (data from triplicates of three independent experiments). **(B–D)** HUAECs were transfected with scrambled siRNA (control) or siRNA directed against $G\alpha_q$ and $G\alpha_{11}$ ($G\alpha_{q/11}$) or Piezo1 and were cultured under static conditions or exposed to disturbed flow in a flow chamber (oscillatory [osc.] flow, 4 dynes/cm^2 at 1 Hz) for the indicated time points. Shown is the mRNA expression of VCAM-1 (B), CCL2 (C), and PDGFB (D) analyzed by quantitative real-time PCR and normalized to human ACTB expression (data from triplicates of three independent experiments). Data represent mean ± SEM; *, P ≤ 0.05; ***, P ≤ 0.001 (one-way ANOVA and Bonferroni's post hoc test).

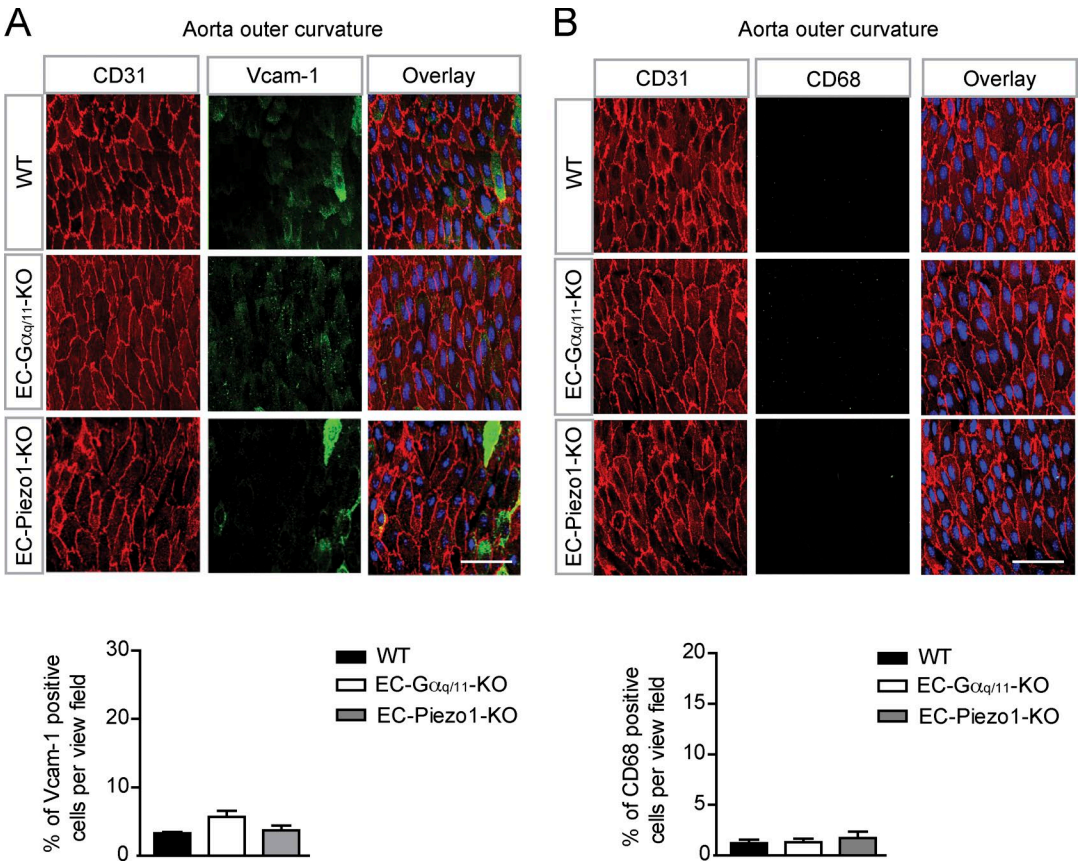

Figure S2. **En face analysis of the aortic outer curvature. (A and B)** Shown are representative en face immuno-confocal microscopy images of the outer curvature. En face aortic arch preparations from 12-wk-old wild-type, endothelium-specific $G\alpha_q/G\alpha_{11}$-KO (EC-$G\alpha_{q/11}$-KO) and Piezo1-KO (EC-Piezo1-KO) mice (n = 6 animal per genotype per condition) were stained with antibodies against CD31, Vcam-1 (A) or CD68 (B) and with DAPI. Immunofluorescence staining was quantified as the percentage of Vcam-1–positive cells among CD31-positive cells per view field (A) or as the percentage of CD68-positive cells per view field (B). Bars, 50 µm. Data represent mean ± SEM (one-way ANOVA and Bonferroni's post hoc test).

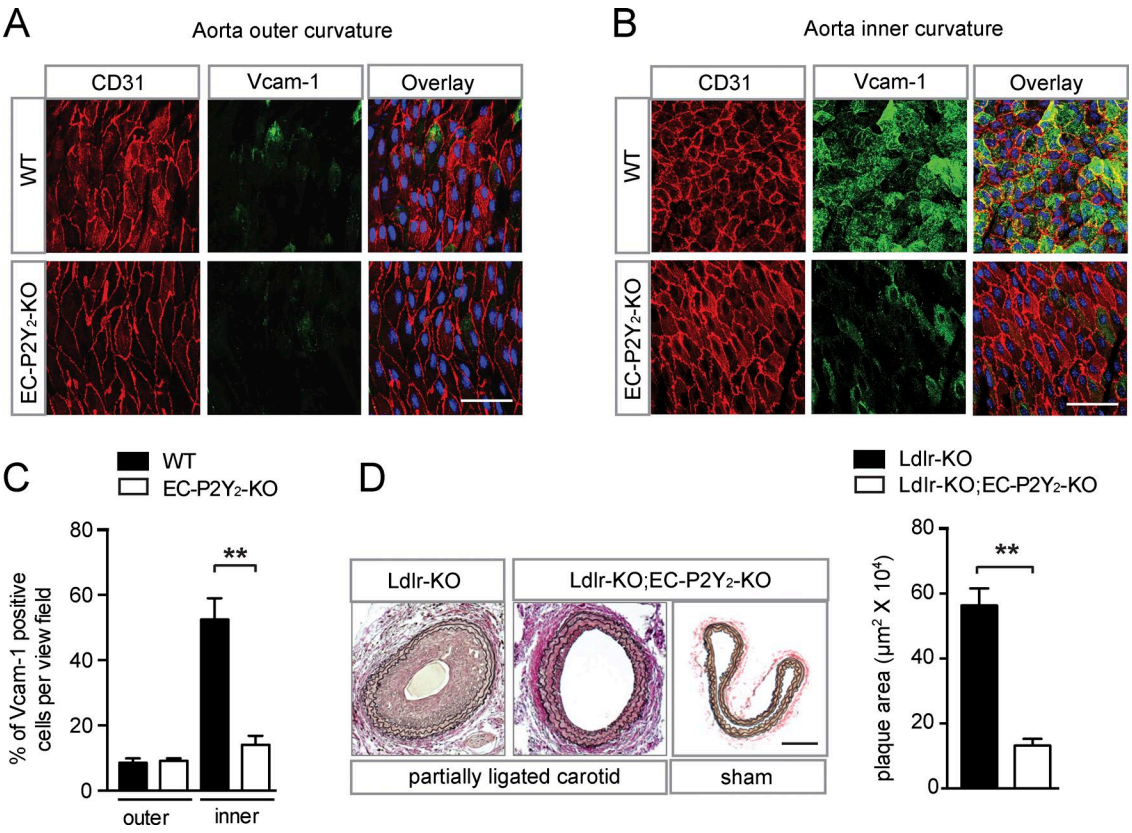

Figure S3. **Analysis of endothelium-specific P2Y2-deficient mice. (A and B)** Representative en face immuno-confocal microscopy image of the outer (A) and inner curvature (B) from 12-wk-old wild-type (control) and endothelium-specific $P2Y_2$-KO mice (EC-P2Y2-KO; n = 5 per genotype). Tissues were stained with anti-CD31 and anti–Vcam-1 antibodies, as well as with DAPI. **(C)** Immunofluorescence staining was quantified as the percentage of Vcam-1–positive cells among CD31-positive cells per view field. **(D)** Ldlr-deficient mice without or with endothelium-specific $P2Y_2$ deficiency (Ldlr-KO;EC-P2Y2-KO) underwent partial ligation of the left carotid artery. 28 d after ligation, carotid arteries were sectioned and stained with elastic stain. Bar diagram shows quantification of the intimal plaque area (n = 6 mice per genotype). Bars, 50 µm. Data represent mean ± SEM; **, P ≤ 0.01 (Student's t test).

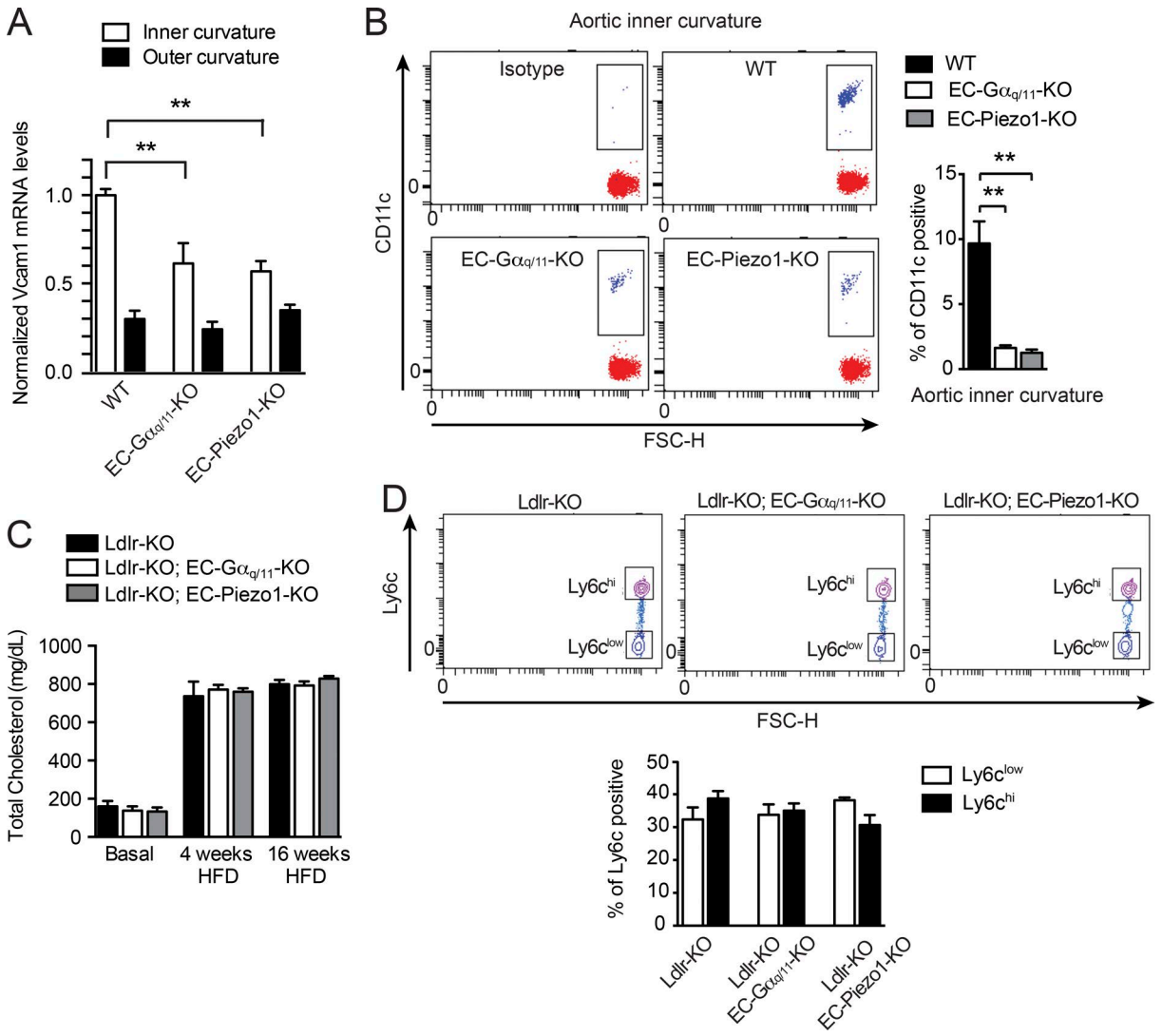

Figure S4. **Endothelial inflammation and atherosclerosis model. (A)** Expression of Vcam-1 mRNA in the intima/subintima of the inner curvature of the aorta from wild-type, EC-Gα_q/Gα_{11}-KO, and EC-Piezo1-KO animals (data from triplicates of three independent experiments; for each experiment two animal samples were pooled; total of six mice per genotype). **(B)** Flow cytometric analysis of live Cd11c-positive cells in the intima/subintima of the inner curvature of the aorta from wild-type, EC-Gα_q/Gα_{11}-KO, and EC-Piezo1-KO animals (total of six mice per genotype). **(C)** Cholesterol levels in the plasma of Ldl-receptor–deficient mice (Ldlr-KO) and Ldlr-KO mice with endothelial cell-specific Gα_q/Gα_{11} deficiency (EC-Gα_q/Gα_{11}-KO) or endothelium-specific Piezo1 deficiency (EC-Piezo1-KO). Six to eight mice per genotype were used. HFD: high-fat diet. **(D)** Levels of Cd45$^+$/Cd11b$^+$/Ly6c^{low} and Cd45$^+$/Cd11b$^+$/Ly6c^{high} cells in the blood of Ldl-receptor–deficient mice (Ldlr-KO), Ldlr-KO; EC-Gαq/Gα11-KO, and Ldlr-KO;EC-Piezo1-KO (total of three to four mice per genotype). Data represent mean ± SEM; **, P ≤ 0.01 (Student's *t* test [A]; one-way ANOVA and Bonferroni's post hoc test [B]).

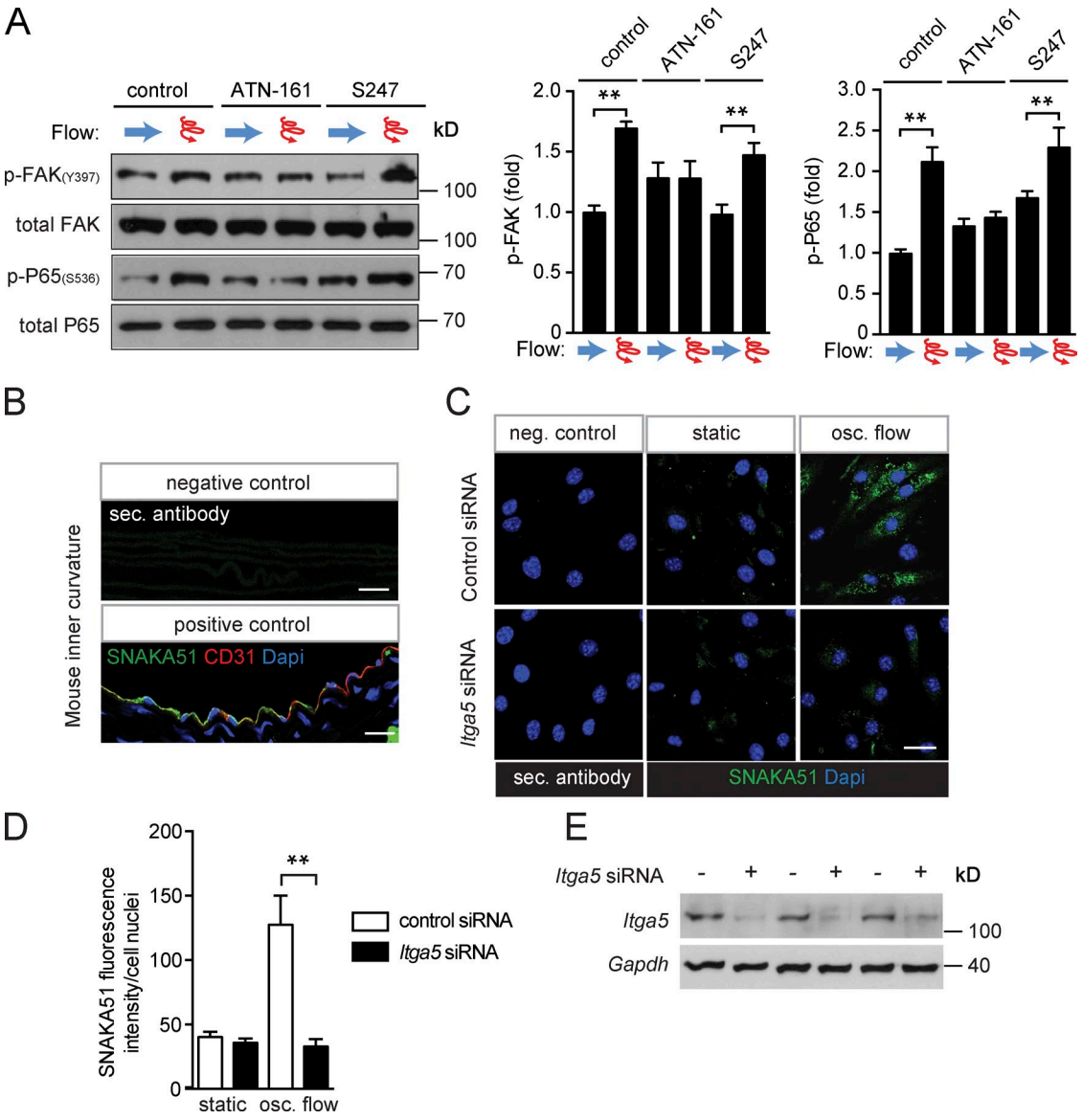

Figure S5. **Integrin α5 is involved in endothelial response to disturbed flow. (A)** HUAECs were incubated with the α5β1 and αvβ3 integrin blocker ATN-161 and S247, respectively, and were exposed to laminar or disturbed flow as described in Fig. 4 A. Activation of integrin signaling was determined by immunoblotting for phosphorylated focal adhesion kinase (pFAK, Y397), and P65 activation was determined by anti–phospho-P65 (S536) antibodies. Bar diagrams show densitometric evaluation of immunoblots (quantification of three to five independent experiments). **(B)** Cross sections of the inner curvature of aortic arches from LDL-receptor–deficient mice fed a high-fat diet for 4 wk were immunostained with SNAKA51, CD31, and DAPI, followed by corresponding labeled secondary antibodies (positive control) or only stained with Alexa Fluor 488– and 594–labeled secondary antibodies (negative control). Shown are representative images of a total of four animals. **(C)** Mouse lung endothelial cells (MLECs) were transfected with control siRNA or with siRNA directed against murine integrin α5 (Itga5) and were kept either under static conditions or were exposed to oscillatory flow for 24 h by the Ibidi flow chamber system. Thereafter cells were immunostained with an antibody against activated α5 integrin (SNAKA51; green) and were stained with DAPI (blue). Negative controls were only incubated with the secondary antibody and DAPI (data of three independent experiments). **(D and E)** Bar diagram (D) shows the quantification of immunocytochemical images and the knock-down efficiency of the siRNA directed against integrin α5, which was analyzed by immunoblotting (E). Data represent mean ± SEM; **, $P \leq 0.01$ (Student's *t* test [A and D]). Bars: 25 µm (B); 50 µm (C).